The energy release rate of mode II fractures in layered snow samples

CHRISTIAN SIGRIST[1,*], JÜRG SCHWEIZER[1], HANS-JAKOB SCHINDLER[2] and JÜRG DUAL[3]

[1]*WSL, Swiss Federal Institute for Snow and Avalanche Research SLF, Flüelastrasse 11, CH-7260 Davos Dorf, Switzerland*
[2]*Mat-Tec AG, Unterer Graben 27, CH-8401 Winterthur, Switzerland*
[3]*Institute of Mechanical Systems, ETH Zürich, Swiss Federal Institute of Technology, CH-8092 Zürich, Switzerland*
Author for correspondence. (E-mail: sigrist@slf.ch)

Abstract. Before a dry snow slab avalanche is released, a shear failure along a weak layer or an interface has to take place. This shear failure disconnects the overlaying slab from the weak layer. A better understanding of this fracture mechanical process, which is a key process in slab avalanche release, is essential for more accurate snow slope stability models. The purpose of this work was to design and to test an experimental set-up for a mode II fracture test with layered snow samples and to find a method to evaluate the interfacial fracture toughness or alternatively the energy release rate in mode II. Beam-shaped specimens were cut out of the layered snow cover, so that they consisted of two homogeneous snow layers separated by a well defined interface. In the cold laboratory 27 specimens were tested using a simple cantilever beam test. The test method proved to be applicable in the laboratory, although the handling of layered samples was delicate. An energy release rate for snow in mode II was calculated numerically with a finite element (FE) model and analytically using an approach for a deeply cracked cantilever beam. An analytical bilayer approach was not suitable. The critical energy release rate G_c was found to be $0.04 \pm 0.02 \, \text{J m}^{-2}$. It was primarily a material property of the weak layer and did not depend on the elastic properties of the two adjacent snow layers. The mixed mode interfacial fracture toughness for a shear fracture along a weak layer estimated from the critical energy release rate was substantially lower than the mode I fracture toughness found for snow of similar density.

Key words: Avalanche formation, cracks in layered materials, energy release rate, interfacial fracture mechanics, snow fracture toughness, snow mechanics.

1. Introduction

Dry snow consists of an ice-matrix filled with air and water vapour. It is a highly porous material (typical relative density: 0.2) with a low specific strength σ/ρ (about 5–$10 \, \text{Nm kg}^{-1}$. Snow exists close to the melting point ($\geqslant 0.95 T_m$) and therefore its microstructure changes continuously and its mechanical properties are strongly temperature dependent. The natural snow cover is layered. Each layer is the result of a snow fall event. The interfaces between the layers – being former snow surfaces – are influenced by the atmosphere. Without these discontinuities in the snow cover there would be no avalanches (Schweizer et al., 2003). The release mechanism of a

dry snow slab avalanche is governed by two successive failure processes. First, damage is accumulated in a weak layer of the snow cover, which leads to a shear fracture spreading out parallel to the slope along the weak layer. (Observations showed that shear fracture can be accompanied by a slope normal displacement of the slab (Johnson et al., 2004; van Herwijnen and Jamieson, 2005) which prompted the development of a fracture propagation model (Heierli, 2005)). Second, a tensile fracture occurs vertical to the slope across the overlaying slab layers (Figure 1), which finally releases the slab avalanche (Perla and LaChapelle, 1970; Schweizer et al., 2003). Both fracture processes can be described and understood by the theory of fracture mechanics. Thus, the corresponding material characteristics, such as the fracture toughness in modes I and II, have to be known (McClung, 1981). They are essential to well-founded and reliable slab release models.

Recently, several studies were made to determine snow fracture toughness in mode I (Kirchner et al., 2000; Faillettaz et al., 2002; Sigrist et al., 2005) and in mode II (Kirchner et al., 2002a, b; Schweizer et al., 2004). For a density of $200\,\mathrm{kg\,m^{-3}}$ a mode I fracture toughness of about $0.5\text{--}1\,\mathrm{kPa\,m^{1/2}}$ was measured, indicating that snow is a very brittle material. All attempts to determine snow fracture toughness in mode II were performed with homogeneous snow samples. However, it is known that shear experiments in homogeneous materials are difficult to perform and cracks tend to change direction, resulting in a pure tensile situation (Anderson, 1995, p. 91).

Shear failures are especially a problem in layered materials (Hutchinson and Suo, 1992). Interfacial fracture mechanics is of importance in many research areas dealing with modern materials such as laminates, fibres and composites. It has also been applied to study natural processes, for example, the icing of electrical transmission cables leading to ice/metal interfaces (Wei et al., 1996). Since snow is a layered material and the layering is a precondition for slab avalanche release, it is essential to test layered samples in mode II.

The crack tip field of an interfacial crack between two dissimilar solids has not the same shape as in a homogeneous material. It can be described with the complex
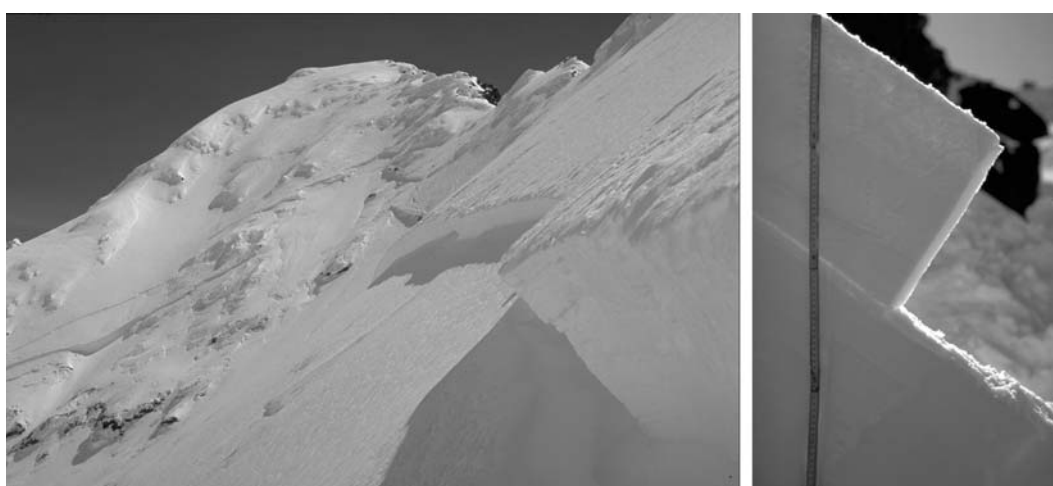

Figure 1. Crown fracture (tensile fracture) of a dry snow slab avalanche (a). Snow cover at the crown of a slab avalanche with a slab on top of a thin weak layer (b) (Schweizer et al., 2003).

interface stress intensity factor $K = K_1 + iK_2$ (Rice, 1988). In this formulation, K_2 describes not only shear stresses but also tensile stresses, i.e. in a bimaterial crack the two modes are coupled and cannot be easily separated. Therefore, we consider the energy release rate G rather than the stress intensity factor K_{II}. From G the absolute value $\sqrt{(K_1^2 + K_2^2)}$ can be derived, but not the components K_1 and K_2. In other words, the energy release rate contains no information about the modes I and II mixing. As we are primarily interested in whether a crack propagates or not, this additional information is not needed.

In this study, layered snow samples of naturally deposited snow were tested in a cold laboratory with the aim to determine the energy release rate of a fracture propagating parallel to the snow layering under shear loading.

2. Experimental procedure

2.1. Sample collection

Snow samples of naturally deposited snow were collected at the Weissfluhjoch (2664 m a.s.l.) above Davos, Switzerland. Beam-shaped aluminium cases of the dimensions $0.5\,\text{m} \times 0.2\,\text{m} \times 0.1\,\text{m}$ were used to cut snow specimens out of the natural snow cover.

To identify weak layers suited for sampling, stability tests were made. We used the compression test (Jamieson, 1999) which involves loading the top of an isolated column of snow (30 cm × 30 cm) by tapping with increasing force. Depending on the number of taps the triggering potential for an avalanche can be estimated as: 0 = very easy, 1–10 = easy, 11–20 = moderate, 21–30 = hard. The aluminium cases were pushed into the snow cover so that the weak layer was caught in the middle of the case, resulting in snow specimens consisting of two more or less homogeneous snow layers separated by a weak layer. A snow profile was made and for each layer grain shape, grain size and snow hardness index according to the International Classification of Seasonal Snow on the Ground (ICSSG) (Colbeck et al., 1990) as well as the snow density ρ were recorded (Table 1). The snow hardness index is a subjective classification with six classes of penetration resistance: Fist (F), Four-fingers (4F), One-finger (1F), Pencil (P), Knife (K) and Ice (I).

The specimens were carried into the cold laboratory at Weissfluhjoch and stored at a temperature of about $-10°C$ for a maximum of 2 days before testing.

2.2. Penetration resistance

Before testing, a SnowMicroPen (SMP) profile was acquired of the uncracked specimen (Figure 2). The SMP is a high-resolution constant speed penetrometer. It records the penetration resistance of a small cone (diameter: 4 mm) which is pushed through the sample perpendicular to the layering of the snow specimen (Schneebeli and Johnston, 1998; Schneebeli et al., 1999). Due to the highly variable snow microstructure, the penetration resistance can even differ for snow of the same density. The SMP resistance profile is appropriate to asses the detailed layering of a snow specimen and allows to derive additional parameters, e.g. the elastic modulus (Johnson and Schneebeli, 1999).

Table 1. Sample characterisation of cold laboratory experiments.

Series	Number	Snow type of weak layer	Snow density (kg/m^3)		Compression test result	Snow temperature (°C)
			(a) upper layer, (b) lower layer	Number of tabs (rating)		
A	8	Faceted crystals and partly surface hoar, 0.75–1.5 mm, F-4F	(a) 267±5 (b) 309±5	12, 12, 12 (moderate)	−9.1	
B	2	Faceted crystals, 0.75–1.5, F-4F	(a) 275±11 (b) 287±2	12, 12, 14 (moderate)	−8.7	
C	10	Mixed forms and partly depth hoar, 0.75–1.5 mm, F	(a) 234±10 (b) 267±10	13 (moderate)	−9.1	
D	7	Mixed forms and partly surface hoar, 1–2 mm, F	(a) 330±6 (b) 348±7	21 (hard)	−9.1	

Summary of type and number of experiments. Snow type is given as grain shape, grain size and hand hardness index according to ICSSG (Colbeck et al., 1990). Snow density is given for the layer above and below the weak layer. Snow temperature refers to the temperature of the snow while testing.
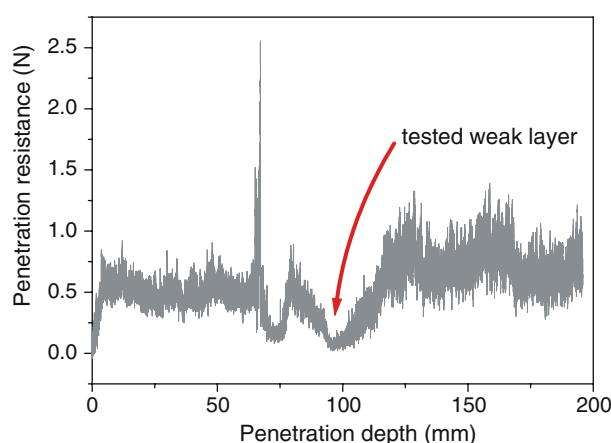

Figure 2. Penetration resistance recorded with a SnowMicroPen for Series B. The weak layer tested in series B was the layer with the lowest penetration resistance at a depth of about 100 mm.

2.3. MODE II FRACTURE TEST

Because the handling of the layered samples was delicate, a simple cantilever beam experiment was chosen. Standard mode II tests, such as the end-node-flexure test or the three-point bend test (Hutchinson and Suo, 1992, p. 114), could not be realised due to the very brittle behaviour of snow.
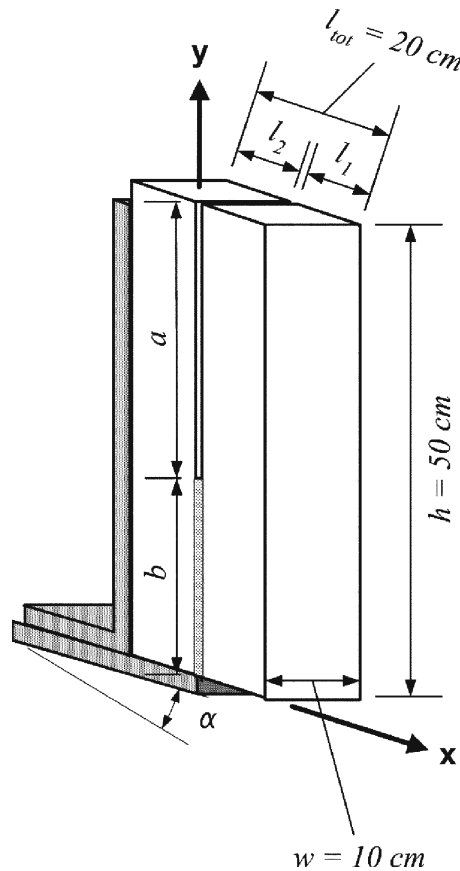
Figure 3. Set-up of the mode II fracture test. The specimen consists of two homogeneous snow layers separated by a weak layer. The snow specimen is iced to an aluminium bar and placed on a table. One layer of length l_2 is supported the other layer of length l_1 is protruding.

All our tests were made in the cold laboratory on Weissfluhjoch at about $-10\,^\circ$C. The mode II fracture test consisted of a notched cantilever beam that was fixed at one end. The layered snow samples were frozen to an aluminium bar in a horizontal position with the lower layer in the snow cover towards the bar. After freezing, the bar was placed in a vertical position on a table, such that the lower layer of the beam with length l_2 was supported by the table (Figure 3). On top of the protruding part, the upper layer in the snow cover, a weight of about 10 N was added in order to increase the shear load and thus to decrease the cut length. With a thin metal saw blade a cut was made along the weak layer from the top towards the bottom until the protruding part of length l_1 broke off under its own weight (Figure 4).

For a cantilever beam the loading of the crack tip is in mixed mode. To maximise the shear component and minimise the tensile component the whole set-up was tilted by an angle α. A minimum tensile load results when the opening moment approximately equals the normal force at the location of the crack tip. The angle α could not be determined exactly because the cut length varied from one experiment to the other. We estimated that for $\alpha \approx 5^\circ$ the tensile stress would be negligibly small.

Figure 4. Series of pictures shot during a mode II fracture test. There is no visible opening of the crack. The mode I component was minimised by tilting the table by an angle $\alpha \approx 5°$.
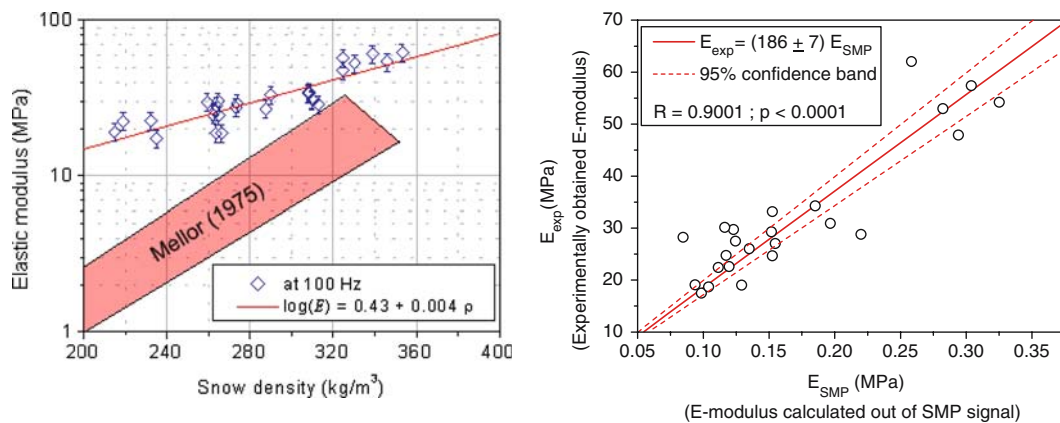

Figure 5. (a) Dynamic elastic modulus in relation to snow density, measured at a frequency of 100 Hz. Range of previous measurements summarised by Mellor (1975) are given for comparison. (b) Comparison between the dynamically measured elastic modulus E_{exp} and the modulus E_{SMP} derived from the penetration resistance signal recorded with the SnowMicroPen.

2.4. ELASTIC MODULUS

To determine the energy release rate G in an interface crack it is crucial to know the elastic modulus (E_1, E_2) of the two involved components (Hutchinson and Suo, 1992). We used a cyclic loading testing device to determine the elastic modulus (Hempel, 2004). Small cylindrical samples cut from the beams with a diameter of 48 mm and a height of 30 mm were tested with a frequency of 100 Hz. The force response due to the predefined deformation was recorded and with the force–displacement information a dynamic elastic modulus was determined. The results are shown in Figure 5a. The measured values were up to a factor of ten higher than previous measurements summarised by Mellor (1975), Shapiro et al. (1997) and more recent measurements by Camponovo and Schweizer (2001). The difference is probably due to the dynamic measurement technique at a relatively high frequency.

Because the cyclic loading experiments were relatively complex and time consuming, the elastic modulus was not measured for each single layer and test sample. Therefore, the SMP penetration resistance signal was used to estimate the elastic modulus (Kronholm, 2004). According to Kronholm (2004), the values of the modulus derived from the SMP signal are too small by a factor of about 150 compared

to previous measurements (Mellor, 1975). Correlating the elastic modulus calculated from the SMP data with the results from the cyclic loading tests resulted in a correction factor of 186 (Figure 5b).

3. Fracture energy

To determine the energy release rate G for our experimental geometry no analytical solution was available. Therefore, we adapted two general analytical approaches to determine G. To overcome some of the limitations of the analytical solutions we compared them to a numerical approach. In the following, the three approaches are described: (1) The analytical cantilever beam approach is valid for deep cracks but assumes a homogeneous material. (2) The analytical bilayer approach assumes two different materials, but an infinitesimally extended specimen. (3) The numerical FE simulation models the experimental set-up consisting of two layers, disregarding the weak layer.

3.1. Cantilever beam with deep crack

The experimental set-up suggests to use a cantilever beam approach to calculate the energy release rate G. Sigrist et al. (2005) used cantilever beams to determine the fracture toughness in mode I with homogeneous snow samples. Since in our case one layer of the specimen was supported and fixed by icing, the fracture energy was assumed to mainly depend on the elastic properties of the protruding layer (E_1). Therefore, the equations derived for a homogeneous material were used as a first approximation, leading to an energy release rate G of

$$G = \frac{K_{\mathrm{I}}^2 + K_{\mathrm{II}}^2}{E_1}. \tag{1}$$

Since the cut lengths in our experiments were deep ($a \geqslant 0.8h$), the system is approximately equivalent to the asymptotic case of a deep edge crack under a bending moment and a shear force:

$$K_{\mathrm{I}} = \frac{c_1 M_{CB}}{b^{3/2}} \tag{2}$$

and

$$K_{\mathrm{II}} = \frac{c_2 P_{CB}}{b^{1/2}}, \tag{3}$$

where b is the ligament length. The constants c_1 and c_2 have to be determined by finite element (FE) modelling and can be set to $c_1 = 3.975, c_2 = 1.463$ for homogeneous samples (Tada et al., 1985). In case of two different materials, c_1 and c_2 may differ from these values depending on the material mismatch. M_{CB} is the norm of the moment due to the weight of the protruding snow layer. In a specimen fixed coordinate system, where the y-axis points along the interface (Figure 3) $\vec{M}_{CB}$ can be written as:

$$\vec{M}_{CB} = \vec{r} \times m\vec{g} = \begin{pmatrix} r_x \\ r_y \\ 0 \end{pmatrix} \times \begin{pmatrix} mg \sin(\alpha) \\ mg \cos(\alpha) \\ 0 \end{pmatrix} = \begin{pmatrix} 0 \\ 0 \\ r_x mg \cos(\alpha) - r_y mg \sin(\alpha) \end{pmatrix}, \tag{4}$$

where $\vec{r}$ is the position vector and m is the mass of the protruding snow layer per specimen width $m = l_1 h \rho$ with l_1 the length of the protruding layer and h its height (Figure 3). g is the gravitational acceleration and α is any rotational angle of the structure. P_{CB} is the loading due to the body weight parallel to the interface

$$P_{CB} = mg \cos(\alpha). \tag{5}$$

Without any additional loading the centre of mass is in the middle of the protruding layer and r_x and r_y can be set to $r_x = l_1/2$ and $r_y = h/2$ (Figure 3). In a more general situation, i.e. when an additional weight is added on top of the protruding part, the centre of mass is lifted towards the additional weight and r_y transforms to

$$r_y = \frac{h}{2} \left(1 + \frac{m_{\text{add}}}{m_{\text{snow}} + m_{\text{add}}} \right), \tag{6}$$

where m_{add} is the mass of the additional weight and m_{snow} the mass of the protruding snow beam. Consequently, the moment M_{CB} as a function of the rotation angle α and the additional weight m_{add} is given as:

$$M_{CB} = (m_{\text{snow}} + m_{\text{add}}) g \left[\cos(\alpha) \frac{l_1}{2} - \sin(\alpha) \frac{h}{2} \left(1 + \frac{m_{\text{add}}}{m_{\text{snow}} + m_{\text{add}}} \right) \right]. \tag{7}$$

3.2. Bilayer with interface crack

Hutchinson and Suo (Suo and Hutchinson, 1990; Hutchinson and Suo, 1992) described an analytical solution for a general interface crack problem. Their aim was to analyse interface cracks between thin films and substrates under fairly general loading conditions (Figure 6). Compared to our experimental set-up with three layers their model only includes two layers. Therefore, we have to consider the weak layer in between the two layers as an interface without lateral extension. The solution for the energy release rate G in plain strain is given by

$$G = \frac{1}{2E_1} \left(\frac{P_1^2}{h} + 12 \frac{M_1^2}{h^3} \right) + \frac{1}{2E_2} \left(\frac{P_2^2}{H} + 12 \frac{M_2^2}{H^3} - \frac{P_3^2}{Ah} - \frac{M_3^2}{Ih^3} \right), \tag{8}$$

where P_i are the applied loads per specimen width and M_i the applied moments per specimen width ($i = 1, 2, 3$). E_1 and E_2 are the elastic moduli of the two components and h, H their heights. $A = \frac{1}{\eta} + \Sigma$ with $\Sigma = \frac{E_1}{E_2}$ and $\eta = \frac{h}{H}$. I is given as

$$I = \Sigma \left[\left(\Delta - \frac{1}{\eta} \right)^2 - \left(\Delta - \frac{1}{\eta} \right) + \frac{1}{3} \right] + \frac{\Delta}{\eta} \left(\Delta - \frac{1}{\eta} \right) + \frac{1}{3\eta^3} \quad \text{with} \quad \Delta = \frac{1 + 2\Sigma\eta + \Sigma\eta^2}{2\eta(1 + \Sigma\eta)}.$$

For our geometry and loading situation (Figure 3) $h = l_1$, $H = l_2$ and we assume P_1 to be the force due to the body weight plus the additional weight that is placed on top of the protruding part, therefore, $P_1 = P_3 = P_{CB}$ (Equation 5). P_2 is zero, M_1 is equal to M_{CB} (Equation 7). M_3 is zero because the specimen is placed on the table at the point where M_3 would act. With these assumptions Equation (8) simplifies to

$$G = \frac{1}{2E_1} \left(\frac{P_{CB}^2}{l_1} + 12 \frac{M_{CB}^2}{l_1^3} \right) + \frac{1}{2E_2} \left(-\frac{P_{CB}^2}{Al_1} + 12 \frac{M_2^2}{l_2^3} \right). \tag{9}$$
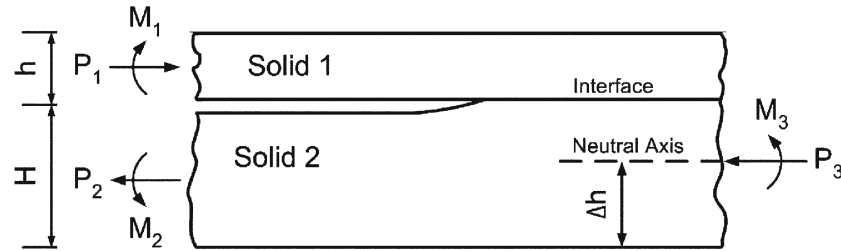
Figure 6. A bilayer material with a half-plane interface crack. After Hutchinson and Suo (1992).

Overall equilibrium of moments provides a constraint so that the moment M_2 can be calculated:

$$M_2 = P_{CB}\left(\frac{l_1}{2} + l_2 - \Delta l_1\right) + M_{CB}. \tag{10}$$

M_2 compensates for the fixed lower edge in our experiments (Figure 6).

3.3. FE MODELLING

Since the analytical solutions did not match our experimental set-up – the deep crack cantilever approach is for a homogeneous material and the bilayer approach is for infinitesimally long specimen – a FE model of the experimental geometry was created to simulate every single experiment. The ANSYS workbench was used. The model calculates the total strain energy E_{st} for a specimen with a cut of length a and with a cut of length $a + da$, where da is an infinitesimal small increase in the cut length ($da/h = 0.004$). The energy release rate G can then be calculated as

$$G = \frac{E_{st}(a + da) - E_{st}(a)}{w \cdot da}, \tag{11}$$

where w is the thickness of the specimen.

To verify the model, the infinitely long thin film of Figure 3 was modelled for which Suo and Hutchinson (1990) had derived an exact analytical solution (Equation 8). The difference between numerical results and analytical solution did not exceed 4% for various loading conditions.

Subsequently, the model was adapted to our experimental geometry (Figure 7). Nodes on the left boundary were fixed in x and y direction, to model the icing of the snow block to the aluminium bar. Nodes on the bottom left boundary were fixed in y direction, corresponding to the support of the specimen on the table. The gravitational acceleration g was implemented, acting with an angle α to the vertical. The additional weight which was placed on top of the protruding snow layer was modelled as a point load.

4. Results and discussion

During winter 2004/2005 four series (A–D) of shear fracture experiments were performed (Table 1). In all series a weak layer was detected by compression tests, observed in a manual snow profile and recorded with the SMP. For the weak layer
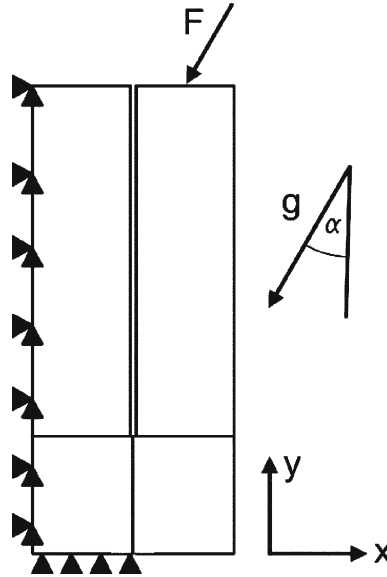
Figure 7. Geometry of the FE model. The black triangles indicate were nodes are fixed in x and/or y direction.

the SMP signal showed a clear decrease in penetration resistance (Figure 2). The weak layer had in most cases a hand hardness index (Fist) that was one step lower than the adjacent layers (Four-fingers to One-finger). For series C, the weak layer was close to a crust. The mean ligament size at failure, $b_c = (h - a_c)$, was 0.08 ± 0.03 m, the mean heights of the two layers l_1, l_2 were: $l_1 = 0.11 \pm 0.02$ m, $l_2 = 0.09 \pm 0.02$ m.

4.1. CRITICAL ENERGY RELEASE RATE

First the results obtained by modelling the experiments with FE will be presented and discussed, because they will serve as basis for the comparison with the analytically obtained results.

For every single experiment an FE simulation was run based on the exact geometry of the experiment. The input parameters were: specimen height, length and thickness (h, l_1, l_2, w), elastic properties of the two layers (E_1, E_2, ν_1, ν_2), density of the two layers (ρ_1, ρ_2) cut length at failure (a_c), as well as angle of rotation (α) and additional weight (m_{add}). The poisons ratio ν_1, ν_2 were calculated in relation to the density $\upsilon = \upsilon_0 + (\rho - \rho_0) \, 5 \times 10^{-4} \, \mathrm{m}^3 \, \mathrm{kg}^{-1}$, with $\upsilon_0 = 0.2$ and $\rho_0 = 300 \, \mathrm{kg} \, \mathrm{m}^{-3}$ according to Mellor (1975). The results for the critical energy release rate G_c for the different series can be seen in Figure 8. G_c is plotted against the elastic mismatch of the two snow layers separated by the weak layer.

The results in Figure 8 suggest that there is no significant dependence of G_c on the elastic mismatch E_1/E_2 between the two layers, or at least a possible trend is smaller than the scatter. The mean critical energy release rate was $G_c = 0.04 \pm 0.02 \, \mathrm{J} \, \mathrm{m}^{-2}$. The findings on metal–ice interfaces showed that even for large changes in E_1/E_2 only slight changes in G_c occurred (Wei et al., 1996). Since for our samples, the difference of the elastic modulus between the two adjacent layers was relatively small,
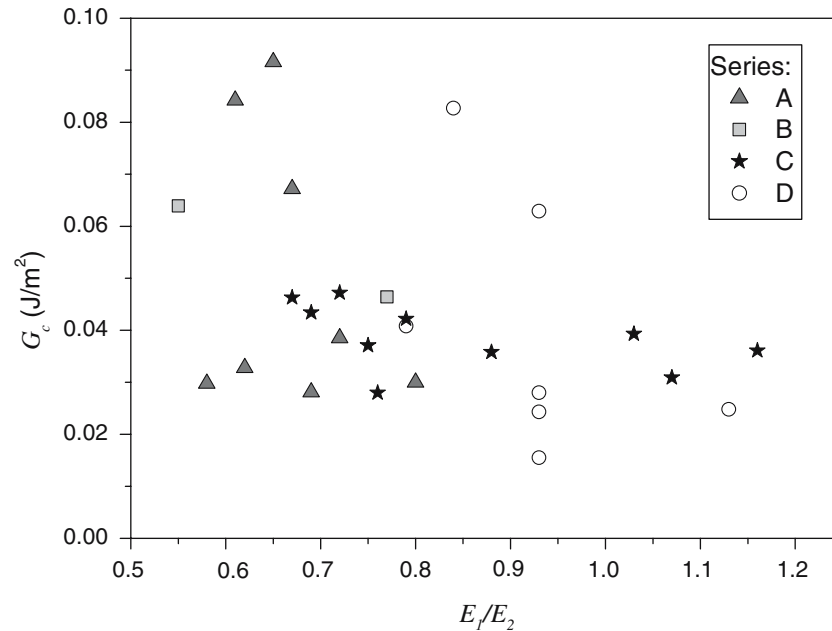
Figure 8. Critical energy release rate G_c in relation to the elastic mismatch E_1/E_2 of the two adjacent snow layers. The results are coded according to the four series of winter 2004/2005.

typically not larger than a factor of two, and the scatter due to the inhomogeneity of the snow and/or due to the experimental method was large, a possible trend might be hidden. Wei et al. (1996) suggested decreasing G_c with increasing mismatch.

The lack of dependence on the mismatch suggests G_c to be primarily a material property of the weak layer than to depend on the properties of the adjacent layers. In other words, the energy needed to destroy the bonds between the weak layer and the adjacent layers seems not to depend on the elastic mismatch between the two layers. This interpretation should be valid as long as the mismatch is not large ($E_1/E_2 \approx \leqslant 10$) which might be the case for most situations in a natural snow cover.

4.2. COMPARISON OF ANALYTICAL AND NUMERICAL RESULTS

In Figure 9 the analytical calculated energy release rates are compared to results from the numerical model. Figure 9a compares the deep crack cantilever approach with the FEM results. The cantilever results were larger, but the values were highly correlated ($R^2 = 0.88$, $N = 27$, $p < 0.0001$). The slope was 0.47 ± 0.01. In Figure 9b the adapted analytical solution for a bilayer material (Suo and Hutchinson, 1990) is compared with the FEM results. No correlation was observed.

The cantilever approach which considers a homogeneous material with a deep crack – in our experiments the ligament length was for most cases smaller than the length of the protruding part $b/l_1 < 1$ – seems to be more appropriate to our experimental geometry than the bilayer solution, even though our samples were layered. The factor of about 0.5 seems to be plausible because the analytical calculation is for a cantilever experiment with free boundary conditions. However, in our experiment one side is fixed and contributes, if at all, only to a limited extent to the energy
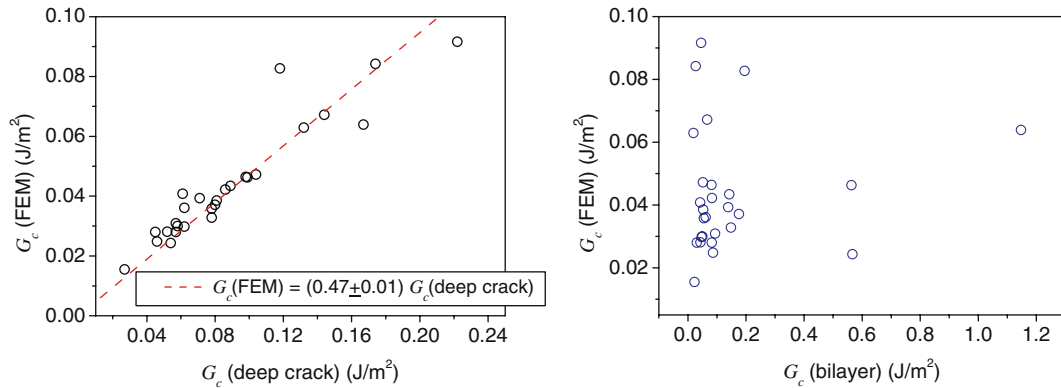
Figure 9. Comparison of the critical energy release rates obtained with the FE model with (a) the deep crack cantilever approach and (b) the bilayer approach of Suo and Hutchinson (1990).
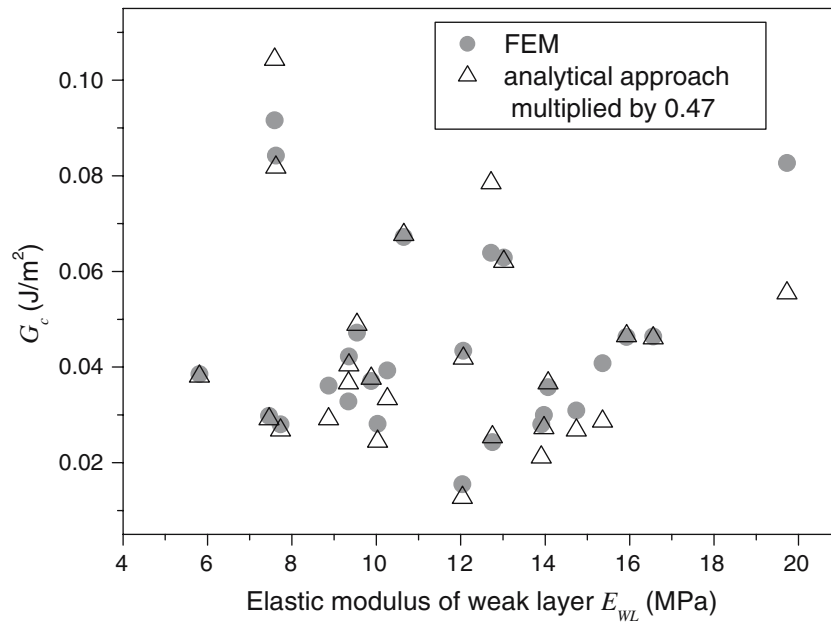

Figure 10. The numerical and analytical (cantilever beam with a deep crack) results for the energy release rate in relation to the elastic modulus of the weak layer E_{WL}. The analytical results are multiplied with a correction factor.

release. The lack of correlation of the bilayer solution was probably due to the finite length of our specimens and due to the large crack length (deep crack situation) for which the bilayer solution is not suited.

With the deep crack cantilever approach of Equation (1) multiplied with a correction factor, we have found an analytical solution to calculate an energy release rate directly from our experimental results without the need of FE modelling. Figure 10 shows the critical energy release rate values of the FEM and the corrected deep crack cantilever solution in relation to the elastic modulus of the weak layer.

Figure 10 suggests that the energy release rate does not depend on the elastic modulus of the weak layer. However, the range of the elastic modulus for the weak layers tested in our experiments was relatively narrow, since the properties of the weak layers were similar for all series (Table 1). For different types of weak layers, i.e. surface hoar, distinctly different elastic moduli are expected. Therefore, we assume that different critical energy release rates would result and it should be possible to determine the critical energy release rate for various weak layer types, as long as the weak layer properties differ significantly so that potential relations of the energy release rate to material properties are not hidden by the inherently large scatter.

A multiple regression for G_c and the elastic moduli E_1, E_2 as well as the elastic modulus of the weak layer E_{WL} did not reveal any statistically significant correlation ($R^2 = 0.15$, $N = 26$, $p = 0.15$).

4.3. COMPARISON WITH MODE I RESULTS

Equation (1) can be used to get a rough estimate of the magnitude of the fracture toughness for our weak layer type: $\sqrt{G E_{WL}} = \sqrt{K_I^2 + K_{II}^2}$. The average weak layer elastic modulus E_{WL} of our samples was 11.6 MPa (Figure 10). The mixed mode interfacial fracture toughness for a shear fracture along a weak layer resulted in $0.49 \pm 0.36 \, \text{kPa} \, \text{m}^{1/2}$ which is about a factor of four lower than the fracture toughness in mode I for samples of similar snow density (Sigrist et al., 2005).

5. Conclusions

Layered snow samples which included a weak layer were tested in shear to determine the energy release rate of a crack propagating along the weak layer:

- A new experimental set-up was tested and proved to be applicable for layered samples.
- The FE method was used to simulate the experiments and determine the energy release rate numerically. For our samples which had a low elastic mismatch, the critical energy release rate $G_c = 0.04 \pm 0.02 \, \text{J} \, \text{m}^{-2}$ did not depend on the elastic mismatch between the two adjacent snow layers. We expect that the critical energy release rate will depend on the weak layer properties.
- Two different analytical approaches were tested and results compared to the numerical FEM results. The analytical approach considering a deeply cracked cantilever experiment with a homogeneous specimen was highly correlated with the results obtained from the FE model. The analytical results were too large by a factor of about 2. An analytical bilayer approach considering two different materials, but an infinitesimally long specimen showed no correlation with the FE results.
- For similar snow densities, mode I fracture toughness results were about four times as large as for the tested weak layers in mode II.

For the future, it will be important to adapt our results on fracture mechanical properties of weak layers to the field and the slope scale. These results will provide much needed input for slab release models including a weak layer.

Acknowledgements

References

Anderson, T.L. (1995). *Fracture Mechanics: Fundamentals and Applications*. CRC Press, Boca Raton, U.S.A., 688 pp.

Camponovo, C. and Schweizer, J. (2001). Rheological measurements of the viscoelastic properties of snow. *Annals of Glaciology* **32**, 44–50.

Colbeck, S. et al. (1990). The international classification for seasonal snow on the ground, International Commission of Snow and Ice of International Association of Scientific Hydrology/prep. by Working group on Snow Classification.

Faillettaz, J., Daudon, D., Bonjean, D. and Louchet, F. (2002). Snow toughness measurements and possible applications to avalanche triggering. in: *Proceedings ISSW 2002. International Snow Science Workshop* (Edited by J.R. Stevens) Penticton BC, Canada, 29 September-4 October 2002, pp. 540–543.

Heierli, J. (2005). Solitary fracture waves in metastable snow stratifications. *Journal of Geophysical Research-Earth Surface* **110**(F2), F02008, doi: 10.1029/2004JF000178.

Hempel, F. (2004). Evaluation of the macro-elastic-modulus of snow, Internal report SLF, Davos.

Hutchinson, J.W. and Suo, Z. (1992). *Mixed-Mode Cracking in Layered Materials, Advances in Applied Mechanics* **29**, 63–191.

Jamieson, J.B. (1999). The compression test – after 25 years. *The Avalanche Review* **18**(1), 10–12.

Johnson, B.C., Jamieson, J.B. and Stewart, R.R. (2004). Seismic measurement of fracture speed in a weak snowpack layer. *Cold Regions Science and Technology* **40**(1–2), 41–45

Johnson, J.B. and Schneebeli, M. (1999). Characterizing the microstructural and micromechanical properties of snow. *Cold Regions Science and Technology* **30**(1–3), 91–100.

Kirchner, H.O.K., Michot, G. and Schweizer, J. (2002a). Fracture toughness of snow in shear and tension. *Scripta Materialia* **46**(6), 425–429.

Kirchner, H.O.K., Michot, G. and Schweizer, J. (2002b). Fracture toughness of snow in shear under friction. *Physical Review E* **66**(2), 027103(3).

Kirchner, H.O.K., Michot, G. and Suzuki, T. (2000). Fracture toughness of snow in tension. *Philosophical Magazine A* **80**(5), 1265–1272.

Kronholm, K. (2004). *Spatial Variability of Snow Mechanical Properties*. University of Zürich, Zürich, 187 pp.

McClung, D.M. (1981). Fracture mechanical models of dry slab avalanche release. *Journal of Geophysical Research* **86**(B11), 10783–10790.

Mellor, M. (1975). A review of basic snow mechanics, Snow mechanics symposium. IAHS-AISH, Vol. 114, Grindelwald, Switzerland, 251–291.

Perla, R. and LaChapelle, E.R. (1970). A theory of snow slab failure. *Journal of Geophysical Research* **75**(36), 7619–7627.

Rice, J.R. (1988). Elastic fracture-mechanics concepts for interfacial cracks. *Journal of Applied Mechanics-Transactions of the ASME* **55**, 98–103.

Schneebeli, M. and Johnson, J.B. (1998). A constant-speed penetrometer for high-resolution snow stratigraphy. *Annals of Glaciology* **26**, 107–111.

Schneebeli, M., Pielmeier, C. and Johnson, J.B. (1999). Measuring snow micro structure and hardness using a high resolution penetrometer. *Cold Regions Science and Technology* **30**(1–3), 101–114.

Schweizer, J., Jamieson, J.B. and Schneebeli, M. (2003). Snow slab avalanche formation. *Reviews of Geophysics* **41**(4), 1016, doi:10.1029/2002RG000123.

Schweizer, J., Michot, G. and Kirchner, H.O.K. (2004). On the fracture toughness of snow. *Annals of Glaciology* **38**, 1–8.

Shapiro, L.H., Johnson, J.B., Sturm, M. and Blaisdell, G.L. (1997). Snow mechanics – Review of the state of knowledge and applications. Report 97-3, US Army CRREL, Hanover, NH, U.S.A.

Sigrist, C., Schweizer, J., Schindler, H.J. and Dual, J. (2005). On size and shape effects in snow fracture toughness measurements. *Cold Regions Science and Technology* **43**(1–2), 24–35.

Suo, Z.G. and Hutchinson, J.W. (1990). Interface Crack between two elastic layers. *International Journal of Fracture* **43**(1), 1–18.

Tada, H., Paris, P.C. and Irwin, G.R. (1985). *The Stress Analysis of Cracks Handbook*. Paris Productions, MO, Saint Louis.

van Herwijnen, A. and Jamieson, B. (2005). High-speed photography of fractures in weak snowpack layers. *Cold Regions Science and Technology* **43**(1–2), 71–82.

Wei, Y., Adamson, R.M. and Dempsey, J.P. (1996). Ice/metal interfaces: fracture energy and fractography. *Journal of Materials Science* **31**, 943–947.